Chapter VII

Using Bird Flight Modes to Enhance Overall Flapping Wing Micro Air Vehicle Performance

Submitted to Bioinspiration and Biomimetics:
W. Thielicke, A.B. Kesel and E.J. Stamhuis
Using bird flight modes to enhance overall flapping wing micro air vehicle performance

ABSTRACT

Birds still outperform existing micro air vehicles (MAVs) in terms of manoeuvrability and energy efficiency. Recent studies on flapping flight in birds, bats and insects have shown that the ability to use unsteady, lift-enhancing mechanisms like the leading-edge vortex are most likely responsible for increased manoeuvrability and slow-flight capability. When flying at higher speeds, endurance and efficiency can be maximized using flapping or gliding flight modes with attached, steady flow. Whereas MAVs that incorporate the use of different aerodynamic mechanisms to increase overall performance are rare, birds combine the advantages of steady and unsteady aerodynamics.

This study presents a flapping wing MAV design that creates lift and thrust with two different aerodynamic mechanisms: In slow-speed flapping flight, lift is generated via unsteady aerodynamics. During faster flight, the MAV has also the ability to intermittently glide efficiently. This combination of flight modes was possible by using rigid wings and wing kinematics based on swifts and swiftlets. Instantaneous and average forces during flapping and gliding were measured at the MAV in a wind tunnel using a 2-axis force balance. Sufficient lift and thrust to overcome gravity and drag were measured for flapping frequencies above 8 Hz. To check the contribution of unsteady aerodynamics in slow-speed flapping flight, aerodynamic lift was modelled using a steady aerodynamics blade-element analysis with parameters derived from kinematics and steady-state force coefficients. The average lift that was observed in direct force measurements exceeds forces predicted by the model by a factor of two. However, when force coefficients that include the extra forces enabled by leading-edge vortices are applied in the blade-element analysis, the result closely matches the direct force measurements. Flapping wings hence offer more aerodynamic possibilities to create forces under a large range of circumstances than fixed or rotary wings: Efficiency or magnitude of force can be maximized when desired; this feature is also very promising for future MAVs that need to complete missions with complex tasks.

INTRODUCTION

In the past decades, a range of different types of micro air vehicles (MAVs) has been developed. The three primarily used techniques, fixed, rotary and flapping wing systems, use different mechanisms to generate lift and thrust. Fixed wing flight is most energy efficient when there is no hover and no slow-flight requirement. Rotary wing aircraft have excellent hovering and manoeuvring performance, but energy efficiency of rotary-wing MAVs is limited (Woods et al., 2001). The third technique uses flapping wings, inspired by insects, birds and bats. Although impressive achievements in this field have been made recently (e. g. Perez-Arancibia et al., 2011; Nakata et al., 2011; De Croon et al., 2012), energy efficiency is still a big challenge (Pesavento & Wang, 2009).

Recent natural disasters have confirmed the need for MAVs that are able to complete demanding rescue and reconnaissance missions. Here, the challenge is to develop aircraft that are manoeuvrable and energy efficient at the same time (Green & Oh, 2005). One suitable approach is to develop hybrid aircraft, that combine the advantages of helicopter and fixed-wing aerodynamics (e. g. Pinder, 2008; Green & Oh, 2009; Itasse et al., 2011, see Chapter V). Another approach to address this challenge is to get inspiration from nature's flapping flyers: Flying animals outperform present MAVs in terms of the necessary combination of manoeuvrability and endurance (Jones et al., 2005). It may therefore pay off to have a closer look at nature's most sophisticated flyers. Most birds are excellent aerial all-rounders. They are useful model organisms for MAVs, as the combination of demanding tasks like take-off, travelling distances, manoeuvring in confined areas and landing is daily practice in most birds.

During gliding and during medium to fast translatory flapping flight, the airflow does not detach from the wings. Wings with a good lift-to-drag ratio (L/D) allow the bird to fly efficiently with relatively low energy expenditure (Norberg, 1990). Slow-speed flapping flight, take-off, landing and manoeuvring have different aerodynamic demands. Insects have been proven to benefit from a lift-enhancing phenomenon called the leading-edge vortex (LEV) during slow and hovering flight with high angles of attack (e. g. Ellington et al., 1996; Birch & Dickinson, 2001). There is no aerodynamic reason why birds should not be able to benefit from the advantages of LEVs, just like insects do (Lentink & Dickinson, 2009). Morphological adaptations in bird wings also hint to the potential importance of additional high-lift mechanisms: The outer part of a bird wing (the hand wing) has very low camber. Additionally, the leading-edge of the hand wing consists of a single vane of one feather and can therefore considered to be sharp (Videler, 2005). Wings with low camber and a sharp leading-edge induce flow separation and are known to facilitate the development of LEVs (Videler et al., 2004, see Chapter III). Several recent studies of gliding and flapping flight of birds and bats (Videler et al., 2004; Muijres et al.,

2008; Hubel & Tropea, 2010; Muijres et al., 2012c; Chang et al., 2013, see Chapters III & IV) give evidence to the conclusion that flow phenomena like the LEV potentially contribute to the necessary extra forces that keep birds aloft in demanding slow-speed flight situations.

The advantages of different aerodynamic mechanisms during different flight modes to create the necessary forces are very promising for application to MAVs. Conventional foil wings of small mechanical flappers which produce mainly thrust during flapping (Lin et al., 2006; Mueller et al., 2009) are not optimized for gliding flight. Therefore, a bio-inspired wing might enable good performance for both flapping and gliding flight modes. Potentially, different flight modes can be employed and the range of possible applications for flapping wing MAVs can be greatly enlarged. A successful implementation would result in flapping wing systems that have an efficient cruise performance and augmented manoeuvrability at the same time.

This study focuses on the development and analysis of a flapping wing model to check the feasibility of the implementation of different flight modes and different aerodynamic mechanisms. The wings are inspired by swiftlets and swifts, bird species with good manoeuvring capabilities and excellent gliding performance (Henningsson & Hedenstroem, 2011). Lift and drag for gliding flight mode and slow-speed flapping flight mode were measured in a wind tunnel. To determine the existence of additional, lift-enhancing flow features in flapping flight, a blade-element analysis was used. Forces were calculated using two different sets of force coefficients. The first set was derived from wind tunnel measurements of steadily translating wings. The existence of force-enhancing flow features in flapping flight is likely, if the blade-element model does not succeed to explain the forces measured during flapping flight (Ellington, 1984a). The second set of coefficients was generated following the leading-edge suction analogy introduced by Polhamus (1966) to include the extra lift enabled by LEVs. If these force coefficients succeed to model the forces that were measured on the MAV, the existence of leading-edge vortices in the flapping wing MAV is most likely.

Studying the forces generated by a flapping wing device in two distinct flight modes can give new ideas for the development of MAVs that are manoeuvrable and energy efficient at the same time.

MATERIALS AND METHODS

MAV PROTOTYPE

The MAV prototype (see Figure 7.1) was designed to be as light as possible in order to check the feasibility of the mechanism in the design-phase already. Two degrees of freedom were implemented in the mechanism for each wing. The wings can flap up and

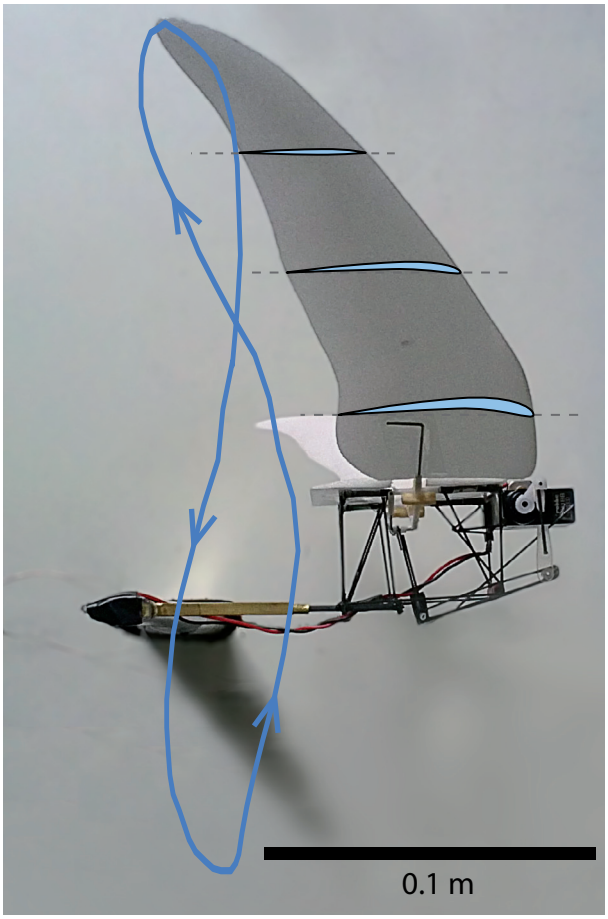

Fig. 7.1: MAV prototype attached to a 2-axes force balance in the wind tunnel. The blue line illustrates a figure-eight wing-tip path. The airfoils of the wing are sketched at three positions.

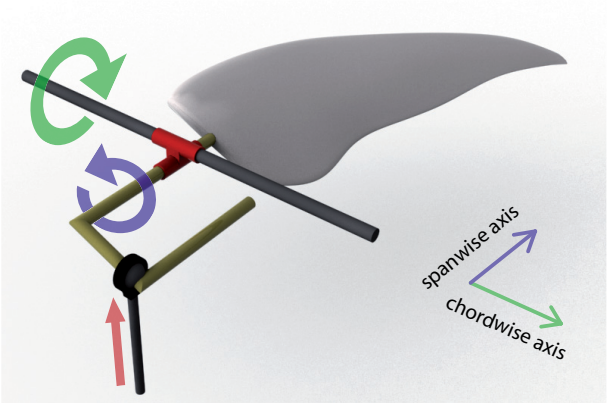

Fig. 7.2: Flapping mechanism. Downstroke action: The pushrod moves up (red arrow) and rotates the wing along the spanwise axis (blue). Subsequently, the wing is pushed down (green) and the downstroke initiates.

down along the chordwise axis and rotate along their spanwise axis (see Figure 7.2). A rotation along the spanwise axis allows for changes in geometric angle of attack at the beat angle extremes. The mechanism mainly consists of two coupled lever arms (see Figure 7.2): When the wing is pushed down, it rotates along its spanwise axis (lowering first the leading-edge). The magnitude of this rotation ('pronation') is limited by a mechanical stop. During the upstroke, the wing rotates in the opposite direction ('supination'); in this case, the rotation is not limited mechanically. The mechanism induces wing rotation at the beat angle extremes and not during the actual up or down stroke. The position of the spanwise joint was selected to be slightly in front of the centre of mass of the wing, which resulted in the desired pronation and supination at the beat angle extremes. A miniature servo motor with modified gear ratio was used to drive the wings and a variable DC power supply to select flapping frequencies between 0 and 9 Hz. The wings are modelled after the wings of swiftlets (*Collocalia linchi*) from 3 mm thick, closed-cell extruded polystyrene foam sheet (DEPRON®). The airfoil at the wing base is cambered and has a round leading-edge, whereas the outer part has a sharp leading-edge and no camber (see Figure 7.1). A total wingspan of 0.33 m and an average chord of 40 mm results in a full span aspect ratio (AR) of 8.3. Similar to the wings of swifts (Savile, 1950; Henningsson et al., 2008), the wings are mostly inflexible. Only some aeroelastic bending near the wing tip was apparent at the higher flapping frequencies. The stroke plane was set to 90° in relation to the oncoming flow. To simulate slow flight situations, flow velocities ranging from 2.28 m/s to 5 m/s were applied in an open jet low speed wind tunnel (test

section diameter = 0.45 m, U_{max} = 14 m/s). The Reynolds number (Re), a measure for the ratio of inertial forces to viscous forces, was calculated following

$$Re = \frac{(\overline{v}_{vert}^2 + U_f^2)^{0.5}\,\overline{c}}{\nu}, \tag{7.1}$$

where $\overline{v}_{vert}$ = mean vertical tip velocity; U_f = free flow velocity; $\overline{c}$ = mean chord; ν = kinematic viscosity.

All measurements were performed for $6.9 \cdot 10^3 < Re < 1.4 \cdot 10^4$. The Strouhal number (St) gives a measure for the ratio of the velocity induced by the flapping wing in relation to the forward flight speed. In the current study, Strouhal numbers in the range of $0.26 < St < 0.72$ were tested in flapping flight. The Strouhal number is given by $St = f A / U_f$, where f = flapping frequency, A = peak-to-peak amplitude of the wing.

KINEMATICS

The geometric angle of attack and the excursion angle of the wing were recorded with the MAV prototype being attached to a force balance inside the wind tunnel. A range of flapping frequencies (3.5 Hz to 9.1 Hz) was tested. As it is difficult to derive the geometric angle of attack directly from image series of the flapping wing, a very thin carbon rod was attached to one wing close to the wing base. Small reflective markers at each end of the rod ensured that changes in projected distance of the markers could be clearly visualized with a high-speed camera (Photron Fastcam APX-RS, focal length = 80 mm, 1000 frames per second, 1/3000 s exposure, 1024 ·1024 pixels resolution) mounted downstream of the flapper. The images were binarized and the reflective markers were tracked automatically with sub-pixel precision for three full flapping cycles with a custom MATLAB tool. The data were used to calculate both the geometric angle of attack (proportional to the arcsine of the projected distance divided by the maximal distance) and the excursion angle over time.

FORCE MEASUREMENT

In gliding flight mode, the lift coefficient (C_L) and the drag coefficient (C_D) were evaluated for geometric angles of attack between -45° and 65°. Lift and drag of single wings were recorded with a 2-axes force balance (for details see Kesel, 2000) at a sampling rate of 1200 Hz. The signal was digitized using an analogue-to-digital converter (Spider 8, Hottinger Baldwin Messtechnik) and processed to derive the force coefficients (MATLAB 7.1, The Mathworks). The wings were tested in gliding flight mode at two Reynolds numbers ($Re = 6.9 \cdot 10^3$ and $1.4 \cdot 10^4$). C_L and C_D were derived via

$$C_L = \frac{2L}{\rho U_f^2 A_{wing}}\ ;\ \text{respectively}\ C_D = \frac{2D}{\rho U_f^2 A_{wing}}\ , \tag{7.2}$$

where L = lift; D = drag; ρ = density; A_{wing} = total wing area.

In flapping flight mode, the horizontal (F_H, 'thrust') and vertical (F_V, 'lift') force components were recorded during eighteen consecutive full flapping cycles, again at 1200 Hz sampling frequency. Several flapping frequencies between 3.5 Hz and 9.1 Hz were tested for three free flow velocities (2.28; 2.57; 2.84 m/s). Re varied between $7.7 \cdot 10^3$ and $1.3 \cdot 10^4$. The mean horizontal force $\overline{F}_H$ and the mean vertical force $\overline{F}_V$ were derived by integrating the instantaneous forces over the wing beat cycle. The non-dimensional mean vertical force coefficient $\overline{C}_V$ was derived by

$$\overline{C}_V = \frac{2\,\overline{F}_V}{\rho\, U_f^2\, A_{wing}} \tag{7.3}$$

BLADE-ELEMENT ANALYSIS

To get insight into the role of lift-enhancing aerodynamic mechanisms, a blade-element analysis and 'quasi-steady' assumptions were used to predict $\overline{F}_V$ and $\overline{F}_H$ of the MAV. The wing planform was digitized and divided into 496 elements along the span wise axis. The effective angle of attack as well as the effective velocity were derived from kinematics and the free flow velocity for each element (Thielicke et al., 2011). Lift and drag of each element was calculated for two different cases using C_L and C_D from two different data sets: The first set (subsequently denominated 'steady' coefficients) consists of lift and drag coefficients that were determined with force measurements of the model wings under steady-flow conditions for a series of angles of attack (-45° to 65°, step = 1°, n = 3). The coefficients were stored in a lookup table, non-integer values were derived by linear interpolation between the neighbouring points. The second set of force coefficients (subsequently denominated 'vortex-enhanced' coefficients), was derived with the relationship between angle of attack and force coefficients as introduced by Polhamus (1966): The total lift of a wing with stably attached LEVs can be approximated as the sum of 'potential-flow lift' and 'vortex lift':

$$C_L = K_p \sin\alpha \cos^2\alpha + K_v \cos\alpha \sin^2\alpha \frac{\alpha}{|\alpha|} + C_{L_o}, \tag{7.4}$$

where α = angle of attack; K_p = constant of proportionality in potential-flow lift term; K_v = constant of proportionality in vortex lift term; C_{L_o} = lift coefficient of the MAV wings at 0° geometric angle of attack.

This theory has successfully been validated with experimental measurements of delta wings with a full-span aspect ratio of up to 4 (Polhamus, 1968). K_p and K_v were determined by Polhamus (1966) for a series of wing aspect ratios using a modified Multhopp lifting-surface theory. The proportionality constants of the most comparable wing geom-

etry were selected (AR = 4; K_p = 3.35; K_v = 3.45). Drag coefficient due to lift is given in Polhamus (1966) as

$$\Delta C_D = C_L \tan \alpha \tag{7.5}$$

The total drag coefficient can be approximated as

$$C_D = \Delta C_D + C_{D_o}, \tag{7.6}$$

where C_{D_o} = zero-lift drag coefficient of the MAV wing.

Lift and drag of each element were integrated for the entire wing and resolved into vertical force F_V and horizontal force F_H. Equivalent to the balance measurements, the instantaneous forces for one wing beat cycle were integrated to derive the mean vertical ($\bar{F}_V$) and the mean horizontal ($\bar{F}_H$) force (for more detailed information, see Thielicke et al., 2011). The results of the blade-element analysis for the 'steady' coefficients and the 'vortex-enhanced' coefficients are compared to the balance measurements of the MAV in flapping flight mode to get further insight into the aerodynamic mechanisms involved.

RESULTS

LIFT AND DRAG IN GLIDING FLIGHT MODE

The balance measurements of the aerodynamic forces in gliding flight mode show the typical characteristics of a wing in steady-flow conditions: Lift increases linearly with angle of attack until the flow detaches from the wings at an angle of about 11° (see Figure 7.3a). Here, the lift coefficient for attached flow is maximal ($C_{L,max} = 1.0 \pm 0.01$ for $Re = 6.9 \cdot 10^3$ and $Re = 1.4 \cdot 10^4$). A further increase in angle of attack ($\alpha > 11°$) results in high additional drag. A maximum lift to drag ratio (L/D) of 8.3 at $\alpha = 5°$ for $Re = 6.9 \cdot 10^3$ and 8.6 at $\alpha = 7.4°$ for $Re = 1.4 \cdot 10^4$ was measured (see Figure 7.3a and 7.4). There is no major difference between the wing polars tested at $Re = 6.9 \cdot 10^3$ and $Re = 1.4 \cdot 10^4$ (see Figure 7.4). C_L and C_D from these steady-flow measurements at $Re = 1.4 \cdot 10^4$ are used as 'steady' coefficients in the blade-element analysis. The 'vortex-enhanced' coefficients are generated using the equations 7.4 to 7.6 given earlier in this chapter. The lift coefficient peaks at 45° angle of attack ($C_{L,max} = 2.6$). The maximal L/D reaches 6.0 for $\alpha = 4°$ (see Figure 7.3b).

FLAPPING FLIGHT MODE

Kinematics

The wing excursion angle and the geometric angle of attack were examined for several flapping frequencies and free flow velocities. Both parameters have a consistent trend in all cases that were analyzed: The wing excursion resembles a sinusoidal oscillation, which is slightly skewed due to different aerodynamic loads during up and downstroke (see Figure 7.5 for two exemplary situations). The wings pronate during the first part of the downstroke which results in a small negative geometric angle of attack (defined as the angle between the wing chord and U_f). The upstroke is linked to a strong supination of the wings. This rotation is initiated just before the start of the upstroke. At elevated flapping frequencies, some instability due to minor oscillation in geometric angle of attack during the upstroke becomes visible (see Figure 7.5b). The total wing amplitude is on average $74.0° \pm 1.2°$ and practically constant (linear regression, slope = −0.19° per Hz, $R^2 = 0.05$) for all flapping frequencies (see Figure 7.6). The maximum degree of pronation (minimum geometric angle of attack) slightly increases with flapping frequency (−2.2° per Hz, $R^2 = 0.89$) as a response to increasing aerodynamic forces in combination with some elasticity in the system (see Figure 7.6). The maximum degree of supination

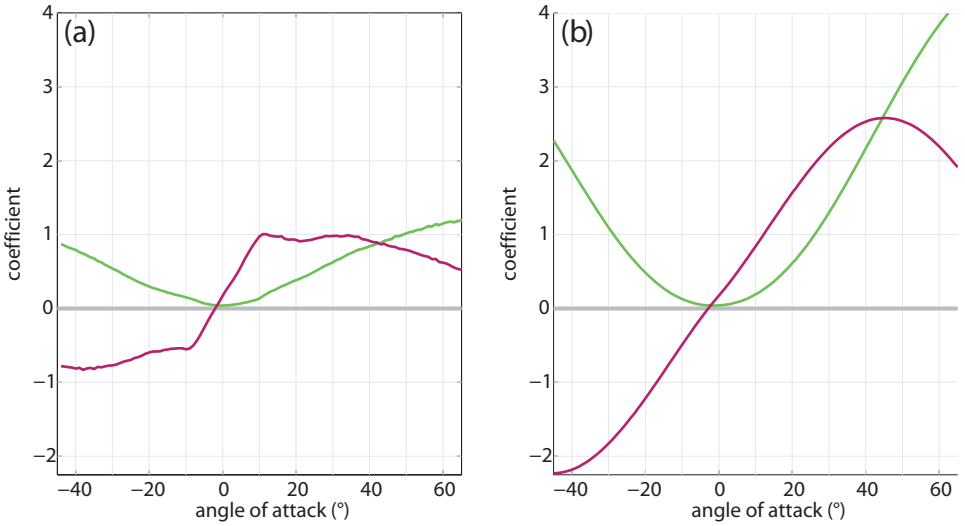

Fig. 7.3: (a) Lift (red) and drag (green) coefficients for the wings in gliding flight mode at $Re = 1.4 \cdot 10^4$. Mean values (n = 3), standard deviation smaller than line width. (b) Lift and drag coefficients following Polhamus (1966)

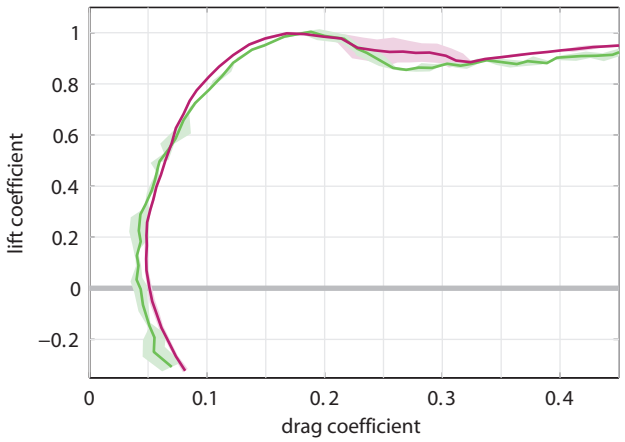

Fig. 7.4: Polar diagram for $Re = 6.9 \cdot 10^3$ (green) and $Re = 1.4 \cdot 10^4$ (red) in gliding flight mode. Mean values (n = 3), standard deviation displayed as shaded area.

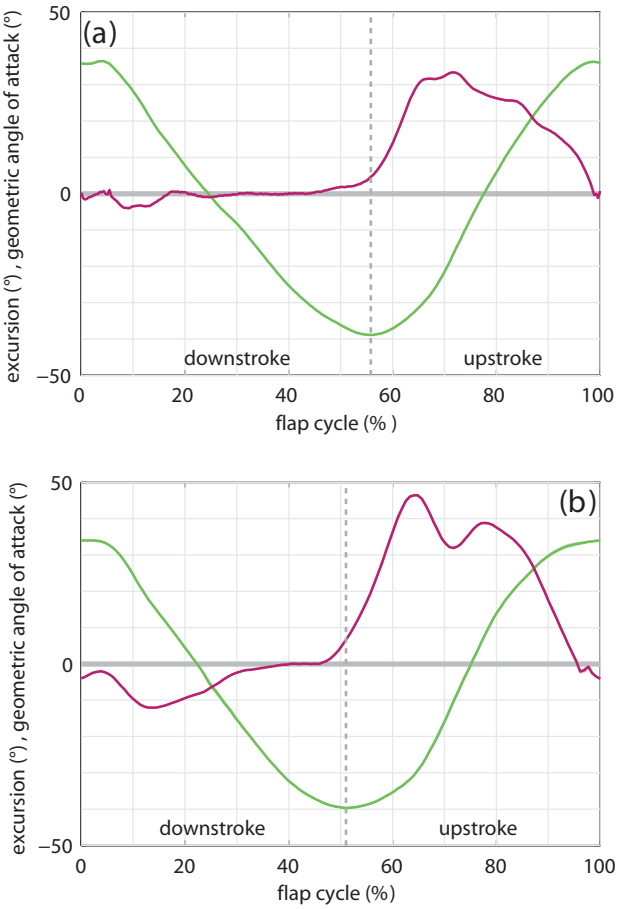

Fig. 7.5: (a) Wing excursion (green) and geometric angle of attack (red) for a flapping frequency of 3.65 Hz and $U_f = 2.28$ m/s. (b) Flapping frequency = 7.61 Hz, $U_f = 2.84$ m/s. Mean values (n = 3), standard deviation smaller than line width.

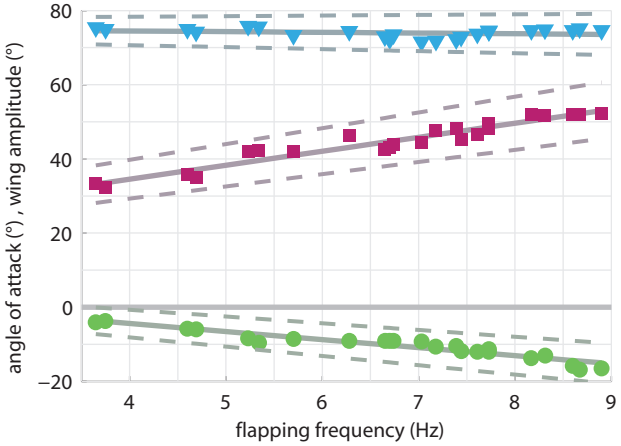

Fig. 7.6: Total wing amplitude (blue triangles), maximum geometric angle of attack during upstroke (red squares) and minimum geometric angle of attack during downstroke (green circles) for all flapping frequencies and flow velocities under test. Linear regression (solid lines, values for R^2 from top to bottom: 0.05; 0.93; 0.89) and prediction bounds with 95% confidence level (dashed lines).

during the upstroke (maximum geometric angle of attack) also depends on flapping frequency. Again, a high flapping frequency increases the amount of supination (3.8° per Hz, $R^2 = 0.93$, see Figure 7.6).

Forces

In flapping flight mode, the MAV creates a resulting force that can be decomposed into a horizontal force component (F_H; 'thrust'), which is parallel to U_f and a vertical force component (F_V; 'lift'), perpendicular to U_f. The MAV creates a positive mean vertical force ($\overline{F}_V$) for all configurations under test. The magnitude of $\overline{F}_V$ increases with St up to a maximum of 95.7 ± 1.4 mN at $St = 0.62$ (see Figure 7.7). An increment of U_f is associated with an increase of $\overline{F}_V$. The mean horizontal force $\overline{F}_H$ is a measure for the 'net thrust' of the MAV. When it equals zero, drag and thrust of the entire MAV system are in balance; in a free flight situation there would be no net horizontal acceleration of the MAV. $\overline{F}_H$ increases with St, following a similar trend as $\overline{F}_V$ (see Figure 7.8). As the free flow velocity increases, the overall drag of the MAV system rises and less 'net thrust' is created (see Figure 7.8). $\overline{F}_H$ exceeds zero for all free flow velocities when St is larger than 0.55 (see Figure 7.8). The non-dimensional mean vertical force coefficient is proportional to the Strouhal number (see Figure 7.9), the maximum $\overline{C}_V$ for the current setup is 1.74 ± 0.02 for $St = 0.71$ and $U_f = 2.57$ m/s. It should be noted that this is substantially higher than the maximum steady-flow lift coefficient ($C_{L,max} = 1.0 \pm 0.01$).

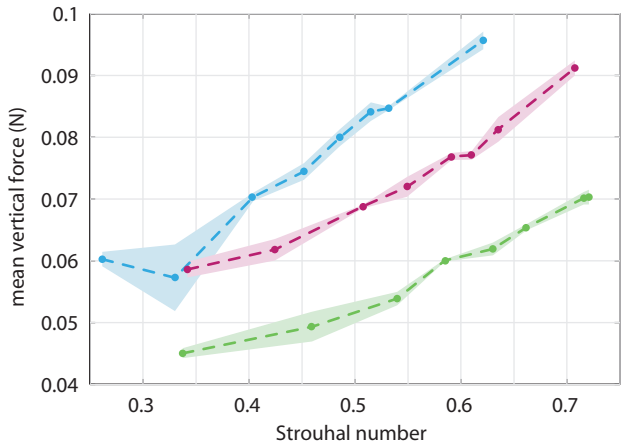

Fig. 7.7: Mean vertical force in flapping flight mode for three flow velocities: 2.28 m/s (green); 2.57 m/s (red); 2.85 m/s (blue). The force increases with St and is larger for increasing $\mathrm{U_f}$. Standard deviation displayed as shaded area.

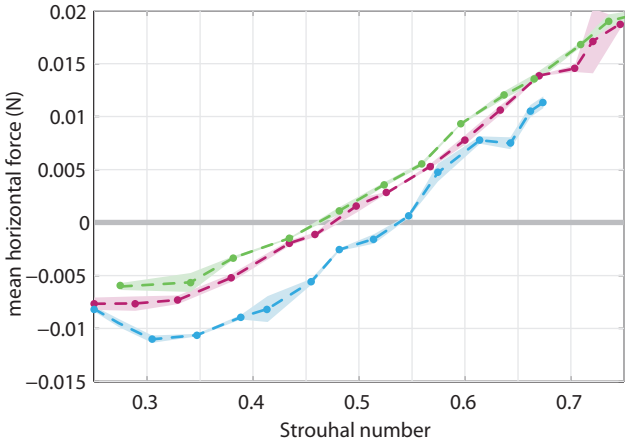

Fig. 7.8: Mean horizontal force in flapping flight mode for different flow velocities: 2.28 m/s (green); 2.57 m/s (red); 2.85 m/s (blue). 'Net thrust' is created when $\mathrm{St} > 0.55$. Standard deviation displayed as shaded area.

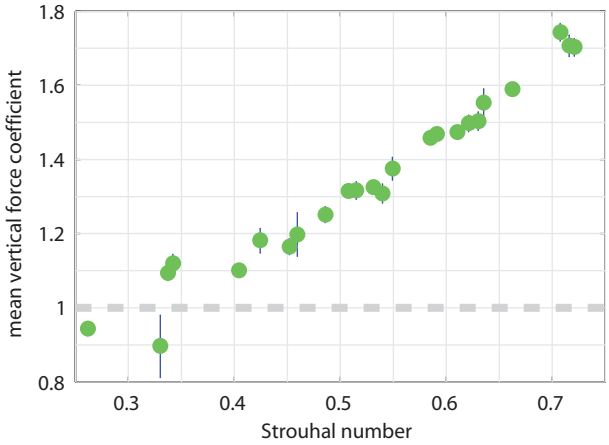

Fig. 7.9: Mean vertical force coefficient vs. St. Data from all free flow velocities was pooled. The vertical force coefficient increases with St, and $\overline{C}_{V,max}$ is substantially higher than $\overline{C}_{L,max}$ in steady-flow conditions (dashed line). Mean values, standard deviation indicated by bars, n = 3.

Blade-element analysis

The magnitude of the mean vertical force calculated with the blade-element analysis using 'steady' coefficients is substantially smaller than the result from the direct force measurement. Particularly at higher St, the difference between the forces measured and the forces modelled with the blade-element analysis becomes increasingly important (see Figure 7.10a): For the maximum St under test the difference in $\overline{F}_V$ reaches -42 mN. In other words, only 55% of the measured lift can be modelled with 'steady' coefficients. There is no such a clear trend for the mean horizontal force. The 'net thrust' is overestimated by the 'steady' coefficients analysis at low St, and underestimated at high St (see Figure 7.10b). When 'vortex-enhanced' coefficients are applied to the blade-element analysis, the results for $\overline{F}_V$ closely match the force balance measurements (maximum deviation = 10 mN, see Figure 7.10a). Expressed as a fraction of the measured mean vertical force, the result of the 'vortex-enhanced' coefficients analysis deviates on average by 2.9% $\pm$ 6.9% (n = 23). The result for the mean horizontal force seems to overestimate $\overline{F}_H$ but the absolute precision of the calculation of $\overline{F}_H$ is comparable to $\overline{F}_V$ (see Figure 7.10b).

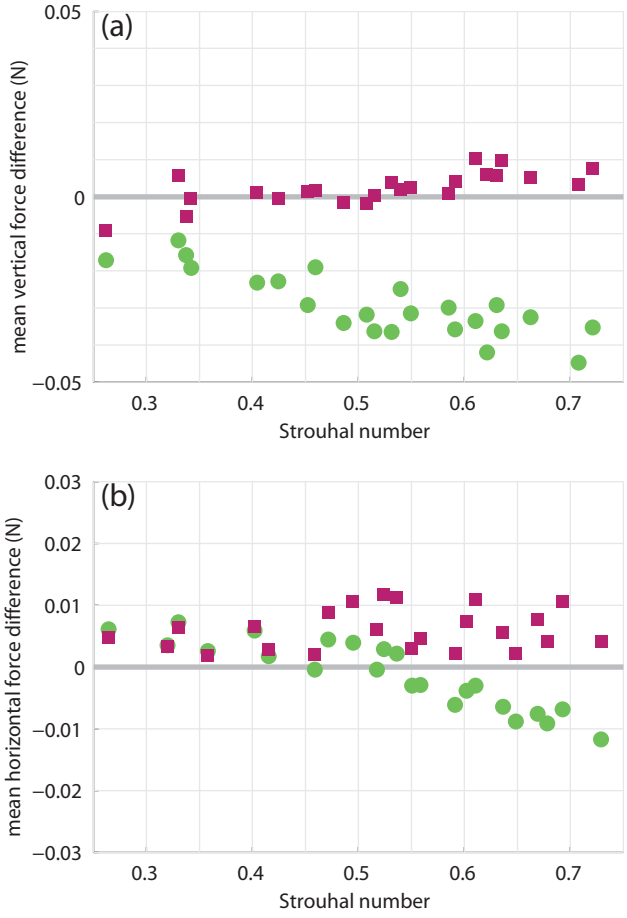

Fig. 7.10: (a) Mean vertical force difference: The force calculated with the blade-element analysis is subtracted from the force measured with the balance. At increasing St, the forces modelled with 'steady' coefficients (green circles) deviate considerably, whereas 'vortex-enhanced' coefficients (red squares) give results that match precisely. (b) Mean horizontal force difference: 'Steady' coefficients overestimate the horizontal force at low St and underestimate at high St. 'Vortex-enhanced' coefficients always overestimate the mean horizontal force.

DISCUSSION

MICRO AIR VEHICLE AND WING KINEMATICS

A MAV prototype that consists of a simple and lightweight mechanism equipped with bio-inspired wings was developed. The mechanism drives the wings by a joint with two degrees of freedom. The geometric angle of attack changes throughout the wing beat cycle, resulting in a large effective angle of attack during downstroke and a small effective angle of attack during the upstroke. The maximal amount of pronation is limited by a somewhat compliant mechanical stop, still pronation increases with flapping frequency. Two factors are responsible for this observation: The main reason for the increase in pronation with flapping frequency is the increase in aerodynamic load. As the centre of lift falls into a region behind the spanwise joint, the aerodynamic load introduces a moment (proportional to angular velocity squared of the wings), that is maximal at mid-downstroke and affects the magnitude of pronation. During the upstroke, the supination is not constrained mechanically; therefore the wings will have to tendency to feather through the flow. The angle will be proportional to the arctangent of the vertical wing velocity divided by U_f. The second reason for the change of kinematics with flapping frequency is inertial force. The analyses of the kinematics have shown that the wings start to supinate just before the upstroke starts. The inertial forces on the wing are proportional to the angular acceleration of the wing (2^{nd} derivative of the excursion angle), and therefore maximal around the reversal points. As the centre of mass of the wings is posterior of the spanwise joint, the angular acceleration creates a moment that initiates wing rotation just before the reversal points are reached. The mechanism hence adapts to changes in flapping frequency: The increase in pronation and supination with flapping frequency causes the system to avoid excessively high effective angles of attack ($\alpha_{eff} > 45°$), preventing C_L to decrease (see Figure 7.3b).

In gliding flight mode, the wings keep a geometric angle of attack of around 0° with respect to the longitudinal axis of the MAV, as the centre of lift of the wings is located behind the spanwise joint. The resulting moment keeps the wings aligned correctly with the MAV without the costs of an extra actuation of the spanwise joint.

Conducting direct force measurements required the MAV to be attached ('tethered') to a force balance. The attachment suppressed any vertical motion of the MAV, but in a free flight situation the chassis would oscillate up and down with a 180° phase shift in relation to the forces created by the wings (sum of aerodynamic and inertial force). This additional velocity component could affect the kinematics and the effective angle of attack and thus the forces created by the MAV. The amplitude of the oscillation can be

assessed using the time-resolved force information from the blade-element analysis and the vertical force caused by wing inertia. Even at the highest flapping frequency tested, the vertical amplitude of the chassis is maximally 24 mm, which is small compared to the total amplitude of the wing tips (200 mm). This will therefore not fundamentally change the aerodynamic situation of the MAV.

GLIDING FLIGHT

The force balance measurements in gliding flight mode reveal a maximum L/D of 8.3 respectively 8.6 and a $C_{L,max}$ of 1.0. A swift in gliding flight at slightly higher Re ($1.8 \cdot 10^4 < Re < 3 \cdot 10^4$) has a maximum L/D ranging from 9.5 up to 12.5 and a maximum lift coefficient of 0.96 (Henningsson & Hedenstroem, 2011). Isolated wings of swifts ($1.2 \cdot 10^4 < Re < 7.7 \cdot 10^4$) perform similarly and have a $C_{L,max}$ of 1.1 (Lentink et al., 2007). Although the wings were tested at lower Re, a similar maximum L/D and lift coefficient was measured. The aerodynamic properties of the wings used in the present study are comparable to the model organism and the MAV prototype has a good performance in gliding flight mode.

FLAPPING FLIGHT

For level flight of the MAV, the mean vertical force needs to equal the gravitational force, and the net horizontal force needs to be larger than or equal to zero. When the prototype is equipped with the appropriate motor, electronics, actuator and battery, the final weight is estimated to be around 9 g. Level flight hence requires a mean vertical force of 88 mN. The measurements show that in slow flight, the MAV is capable of creating a mean vertical force of up to 95.7 ± 1.4 mN. At the same time it creates a net thrust of 7.8 ± 0.4 mN. In slow-speed flapping flight mode, the MAV prototype hence creates sufficient vertical and horizontal force for level flight.

The time-resolved blade-element analysis provides some insight into the role of the up and downstroke. Most of the vertical force is generated during the downstroke. The magnitude increases from base to tip (see Figure 7.11a), as the effective angle of attack and the resulting velocity both increase with span. The wings create thrust during the downstroke although the magnitude is relatively small compared to the vertical force component. During the upstroke, the use of relatively rigid, untwisted wings has a noticeable effect on the distribution of the vertical force and thrust: The wing base operates at a positive effective angle of attack and generates a positive vertical force and negative thrust of comparable magnitude. Further to the wing tip, the effective angle of attack gradually decreases and is finally inverted. The wing creates negative vertical force and positive thrust (see Figure 7.11b). Accordingly, 'lift' and thrust during slow-speed flight are not created at a constant rate throughout the flapping cycle. The forces have a periodic pattern, which is in contrast with conventional rotary wing MAVs, that might

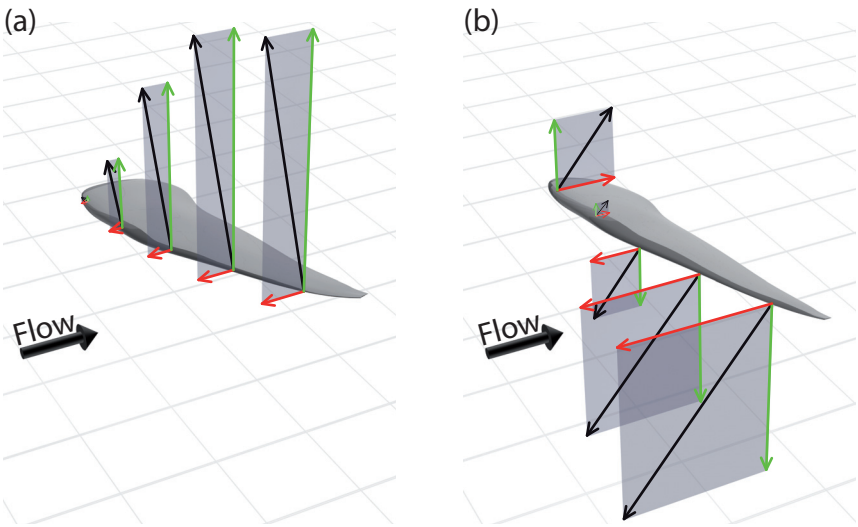

Fig. 7.11: Blade element analysis, force situation at mid-up and mid-downstroke. (a) mid-downstroke. 'Lift' (green arrows) and thrust (red arrows) increases toward the wing tip. (b) mid-upstroke. The outer part of the wing creates negative 'lift' and positive thrust. The inner part of the wing creates positive 'lift' and drag. All vectors drawn to scale, $St \approx 0.5$, $U_f = 2.57$ m/s.

also have a superior efficiency in hovering flight (e. g. Hall & Hall, 2001; Usherwood, 2009). Provided that the mean forces of a rotary wing and a flapping wing are equal, a flapping wing therefore creates much higher peak forces. For slow-speed manoeuvring of birds in flapping flight, the aerodynamic mechanisms create large and rapidly alternating forces (Warrick et al., 2002). Using flapping-wings as propulsion might be advantageous in terms of manoeuvrability (Usherwood, 2009), and the ability to create large peak forces may increase agility.

THE INFLUENCE OF THE DELAYED STALL

As noted earlier, the maximum lift coefficient under steady-flow conditions is 1.0 ± 0.01. At relatively low Strouhal numbers ($St < 0.4$), the mean vertical force coefficient in flapping flight is similar to the $C_{L,max}$ under steady-flow conditions (see Figure 7.9), indicating that the wings perform similarly in flapping flight and in steady-state gliding flight. Low St are typical for birds during efficient cruising flight, where it is expected that LEVs do most likely not develop on the wings (Taylor et al., 2003). The data of the present study supports this idea. At higher St however, the value for $C_{L,max}$ under steady-flow conditions is readily exceeded in flapping flight mode. The mean vertical force coefficient peaks at 1.74 ± 0.02 at a Strouhal number of 0.71. Such an increase

of the force coefficient during flapping is likely to be associated with the delayed stall, respectively the development of a LEV (Kim et al., 2009). The results of the blade-element analyses show the importance of enhanced force coefficients in flapping flight at higher St. It was shown that the blade-element analysis using steady-state force coefficients is not suitable for modelling flapping flight at elevated Strouhal number, where the influence of the delayed stall increases (Nudds et al., 2004). 'Vortex-enhanced' coefficients have a significantly higher C_L and C_D magnitude, and can approximate the forces measured in flapping flight. The leading-edge vortex is the most prominent flow phenomenon of the delayed stall. It is known to augment aerodynamic forces in delta wings (e. g. Wu et al., 1991) and in flapping wings of (robotic) insects (e. g. Ellington et al., 1996; Birch & Dickinson, 2001), bats (Muijres et al., 2008), birds (Hubel & Tropea, 2010; Muijres et al., 2012c) and MAVs (e. g. Takahashi et al., 2010; Tanaka & Shimoyama, 2010; Nakata et al., 2011). In an earlier study (Thielicke, 2007), the same type of flapping wing as in the present study was used during flow visualization. The kinematics as well as the Reynolds number and Strouhal number were very similar. Ink was released from the wing to demonstrate the existence of a prominent and stable LEV that instantly developed with the onset of the downstroke (see Figure 7.12). The focus of the present study is on force measurements. Nonetheless, the importance of LEVs for the MAV is confirmed with the increase in vertical force coefficient, the success of the 'vortex-enhanced' blade-element analysis and the flow analysis of the same wing type in a previous study.

MICRO AIR VEHICLE PERFORMANCE ENHANCED BY BIRD FLIGHT MODES?

Which capabilities define the 'optimal' MAV? One of the main fields of current research is the development of MAVs for complex missions: These missions require the MAV to reach a remote location that is potentially far away from the starting point. Subsequently, the area or the building has to be explored and measurements are taken (Green & Oh, 2009; Itasse et al., 2011). These tasks require MAVs that are energy efficient and have an enhanced manoeuvrability at the same time. A combination of the advantages of fixed wing and rotary wing MAVs is therefore necessary.

The concept proposed in the current study enables such a combination by using two different flight modes. Slow-speed flapping flight is enabled by LEVs which augment the aerodynamic forces. These slow flight capabilities will greatly improve manoeuvrability in confined areas or in indoor locations, as turning radius decreases with flight speed. The efficiency of generating lift via LEVs at high St is supposed to be inferior to fully attached flow aerodynamics due to an increase in drag (Taylor et al., 2003). However, in slow speed, high angle of attack situations like take-off, landing and manoeuvring, the sheer presence of a reliable and maximal force is relatively more important than energy efficiency. The power requirement of a flapping wing device that benefits from leading-edge vortices to augment lift in slow-speed flight is about 132 W/kg (Lentink et al., 2009). This is not fundamentally different from the power requirement of up to

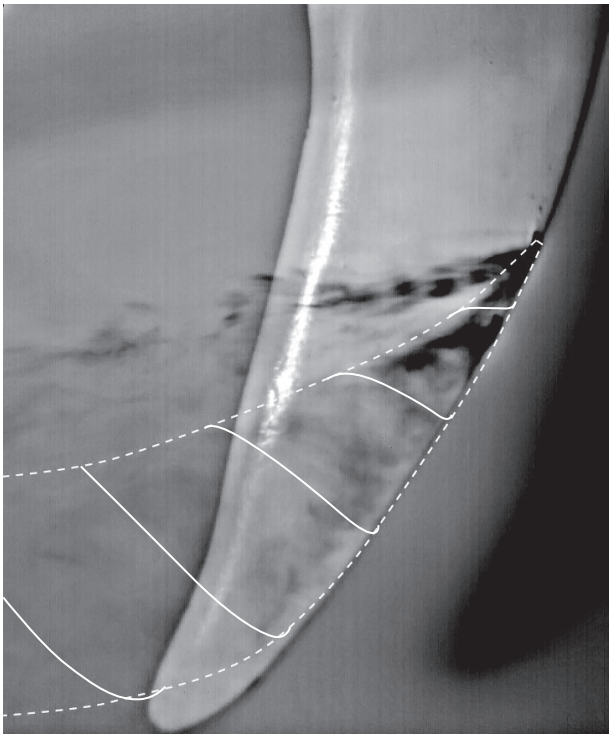

Fig. 7.12: Ink is released at the leading-edge of a flapping wing at mid-downstroke and visualizes a LEV (emphasized with white lines, data from Thielicke (2007)).

date multirotor systems (123 to 243 W/kg, W.T., unpublished observation). Flapping flight might therefore present a suitable alternative to conventional rotary wing MAVs.

The power requirement in flapping flight mode potentially decreases with flight speed. In cruising flight, at higher velocities and lower St, it is likely that LEVs do not develop on flapping wings (Taylor et al., 2003). Here, exceptionally high force coefficients are not necessary (Nudds et al., 2004), and the presence of fully attached flow aerodynamics increases efficiency. This is demonstrated by the low power requirement of a flapping wing MAV designed to perform cruising flight at low St with fully attached flow (63 W/kg, FESTO, 2011).

The second flight mode that was tested – gliding flight – is suitable for the mission parts where energy efficiency is most important and manoeuvrability is of second interest. The efficiency is directly related to the L/D of the wings, and optimizing the L/D is hence important. Gliding flight represents the ultimate flight mode to stay airborne without investing much energy (Videler, 2005), and future MAVs might even benefit from thermal updrafts (Akos et al., 2010) or soar upwind of urban buildings to regain height (White et al., 2012).

The efficiency of flapping wing MAVs in cruising flight might be further improved – and may finally reach the superior cruising efficiency of fixed wing MAVs – by using a flight strategy that combines different flight modes. Such a flight strategy is used by many medium-sized birds that alternate between gliding flight phases and bursts of flapping flight (intermittent flight). This behaviour is assumed to reduce mechanical power output relative to continuous flapping flight (Rayner, 1985; Rayner et al., 2001; Tobalske, 2001). It appears that many birds that potentially have a good gliding performance use this strategy (Tobalske, 2001). Swifts – which are used as example for modelling the wings – have an exceptional gliding performance, when using L/D as benchmark (Henningsson & Hedenstroem, 2011). Model estimations suppose that these birds species can save up to 15% energy when alternating between gliding flight and flapping flight (Muijres et al., 2012a).

CONCLUSIONS

The aim of this study is to show the potential of flapping wing MAVs using different flight modes as in birds. The benefits that arise from the specific aerodynamic properties of flapping wings were discussed. However, there are still remaining challenges on the way to a flapping wing MAV that can benefit from bird flight modes. The wings have to adapt to the flight mode in order to have larger effective angles of attack at slow speed flight, and lower effective angles of attack during cruising and gliding flight to ensure energy efficiency. Research on adaptive wings, such as membrane wings with adjustable camber, has already been started (e. g. Kim et al., 2009). Additionally, there are control, actuation and manufacturing issues that still need to be solved for flapping wing MAVs. Control strategies for MAVs are currently making huge progress. For instance, the demanding 'perching' manoeuvre of birds was already implemented in fixed wing MAVs (Roberts et al., 2009; Desbiens & Cutkosky, 2009), enhancing the applicability of these miniature aircraft for e. g. surveillance tasks.

Flapping wing MAVs that benefit from bird flight modes and strategies can be a promising solution for tasks consisting of covering a distance and manoeuvring in small or confined areas with just one single device. They might soon become the biologically inspired alternative to hybrid MAVs like tilt-bodies and tilt-wings when the advances in available technology continue to evolve rapidly.